nature sustainability

Article

https://doi.org/10.1038/s41893-026-01975-9

Widespread North American pollution and health impacts from early twentieth century copper production

Received: 27 March 2026

Accepted: 28 September 2026

Published online: 10 November 2026

Check for updates

Joseph R. McConnell[1] ✉, Nathan J. Chellman[1], Sophie M. Wensman[1], Alison S. Criscitiello[2], Andreas Plach[3,4,5], Dorthe Dahl-Jensen[6,7], Diedrich Fritzsche[8], Kira M. Holland[2], Drake McCrimmon[1], Matthew B. Osman[9], John Sandlos[10] & Andreas Stohl[3]

Rapid expansion of fossil-fuel burning and base-metal production during the Second Industrial Revolution resulted in widespread pollution and potentially important health impacts. Here we used an array of Arctic ice cores, atmospheric modelling and epidemiology to investigate arsenic and other toxic heavy metal pollution. From multiple lines of evidence, we attribute the observed 1884–1918 increases of up to 15-fold in arsenic and other heavy metals primarily to emissions from copper production at Anaconda, Montana—then among the world's largest copper producers and a well-documented source of arsenic emissions. We estimate emissions from Anaconda of 11 and 4.4 kt yr^{-1} for arsenic and lead, respectively, during the two decades of peak production that polluted much of North America. Installation of electrostatic precipitators, delayed for a decade by lax regulation, reduced heavy metal emissions by 65%, but not before exposing millions of Americans to cancer risks, cognitive declines and other ailments.

Arctic and near-Arctic ice core records show that deposition of many toxic heavy metals and other pollutants across large regions of the Arctic was substantially higher during the late nineteenth and early twentieth centuries[1–3] than at any time during the past 170 years (Fig. 1). This period included the ~1870 to ~1914 Second Industrial Revolution (hereafter referred to as the Industrial Revolution) when widespread exploitation of many natural resources including fossil fuels and base metals such as copper (Cu), nickel (Ni), zinc (Zn) and lead (Pb) rapidly expanded, leading to pronounced increases in air pollution especially in North America (NA) and Europe. Following the Great Depression (1930–1935), resource exploitation and industrial output accelerated, resulting in increased atmospheric emissions of toxic substances through at least the early 1970s when regulatory policies such as the US Clean Air Act were first implemented. It is therefore contrary to expectations that the emissions of certain toxic heavy metal pollutants peaked in the early twentieth century.

Arsenic (As) and Pb are among the heavy metal pollutants most toxic to humans and ecosystems; the World Health Organization recommends no safe levels of exposure[4]. Based on their frequency of occurrence, toxicity and potential for human exposure, As and Pb are respectively first and second on the Agency for Toxic Substances and Disease Registry Substance Priory List, ahead of mercury (Hg) and other well-known highly toxic substances. Acute and chronic exposure to elemental As and its associated compounds, sometimes referred to as the 'king of poisons', have been linked to increased risk of cancer, neural complications, diabetes and other serious diseases[5,6]. Dangerous

[1]Division of Hydrologic Sciences, Desert Research Institute, Reno, NV, USA. [2]Department of Earth and Atmospheric Sciences, University of Alberta, Edmonton, Alberta, Canada. [3]Department of Meteorology and Geophysics, University of Vienna, Vienna, Austria. [4]Department of Meteorology, Stockholm University, Stockholm, Sweden. [5]Bolin Centre for Climate Research, Stockholm University, Stockholm, Sweden. [6]Niels Bohr Institute, University of Copenhagen, Copenhagen, Denmark. [7]Centre for Earth Observation Science, University of Manitoba, Winnipeg, Manitoba, Canada. [8]Alfred-Wegener-Institut Helmholtz-Zentrum für Polar-und Meeresforschung, Potsdam, Germany. [9]Department of Geography, University of Cambridge, Cambridge, UK. [10]Department of History, Memorial University of Newfoundland, St John's, Newfoundland and Labrador, Canada. ✉e-mail: Joe.McConnell@dri.edu

https://doi.org/10.1038/s41893-026-01975-9

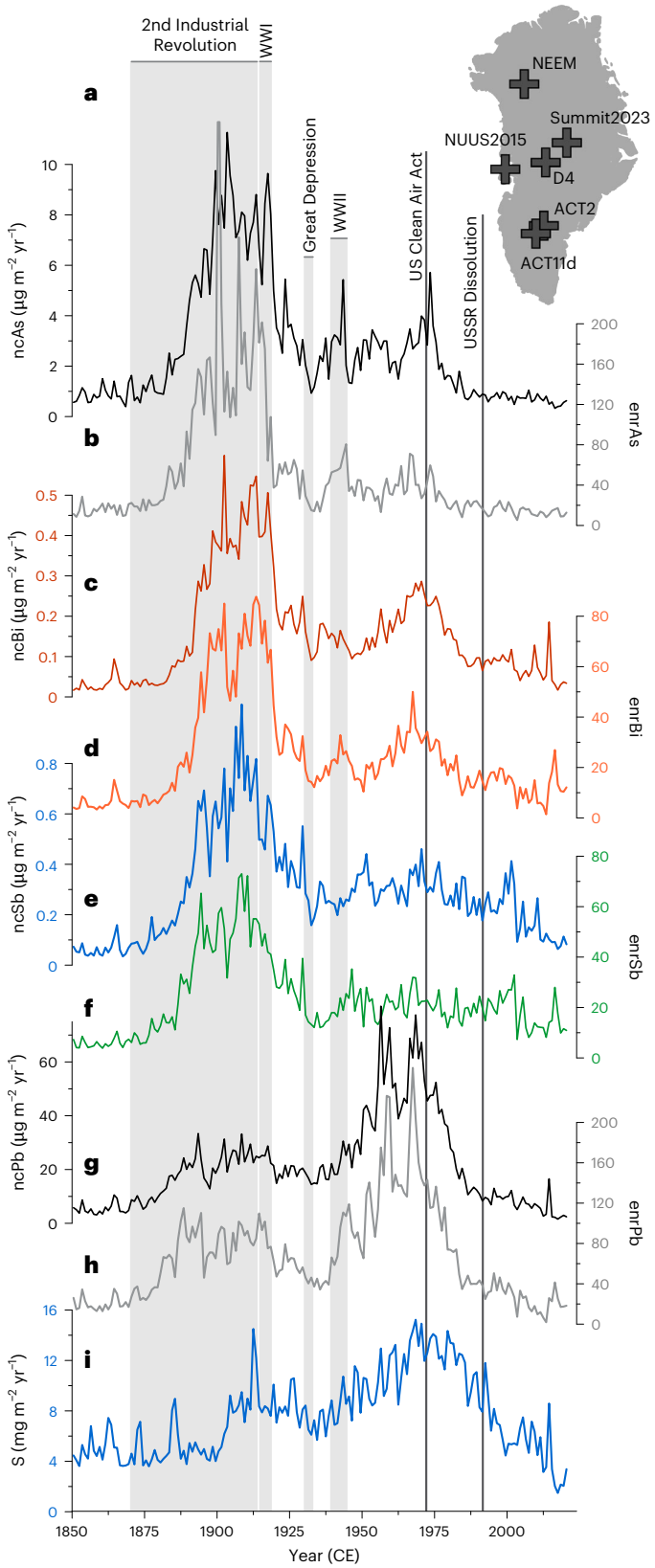


Fig. 1 | Western Greenland heavy metal and sulfur pollution from 1850 to 2020. **a**,**b**, ncAs deposition and As enrichment at Summit, Greenland. **c**–**i**, Deposition (left axis) and enrichment (right axis) of ncBi, ncSb and ncPb, and sulfur deposition (**i**) in a six-core western Greenland composite (WGC, inset). Dates of major relevant historical events are shown.

levels of As exposure are associated with industrial pollution generated primarily by metal production, particularly Cu and other non-ferrous smelting of sulfide ores[7], and coal burning. The severely detrimental effects of Pb exposure in humans during recent decades are well known, with infants and children especially vulnerable[8].

Glacier ice contains the best indirect record of past atmospheric constituents, and ice core studies have examined the magnitude and sources of heavy metals during recent centuries and millennia (for example, refs. 2,9–15). Because of the short atmospheric lifetimes (typically days to weeks), concentrations and deposition rates of pollutants such as As, Pb[2,11,16,17], sulfate (for example, ref. 18) and refractory black carbon[19–23] vary rapidly in both space and time, thereby necessitating spatial arrays of observations to understand past sources, concentrations and exposure levels. Although recent Arctic Pb pollution has been documented clearly in ice cores[2,9,14,16,24,25], very few ice core As records have been reported, and those that exist are hampered by low temporal resolution and sparse geographic distribution[3,26].

Here we used chemical and isotopic measurements in an Arctic-wide array of ten high-depth-resolution, well-dated ice core records from Canada, Greenland and the Russian Arctic (Extended Data Table 1) to assess the timing, magnitude and likely sources of As, Pb, bismuth (Bi) and antimony (Sb) pollution in the higher-latitude Northern Hemisphere. All four metals or metalloids are found in varying proportions in ferrous and non-ferrous ores and fossil fuels. They are volatile and are thus often co-emitted from industrial processes. We focused particularly on the 1850–1950 period extending from well before to well after the Second Industrial Revolution of 1870–1914. Measurements were made using the unique, well-established continuous ice core analytical system at the Desert Research Institute (DRI)[27,28]. Non-crustal components (for example, ncAs), enrichments relative to crustal dust (for example, enrAs), as well as depositional fluxes, were calculated following standard procedures (Methods)[1]. Following recent methods development, four of the ten cores included As measurements (Extended Data Table 1). Taking advantage of similar variability and consistent concentration ratios between ncBi and ncAs during and immediately after the Industrial Revolution (Extended Data Fig. 1), however, we used ncBi measurements in the remaining six cores as proxies to extend As deposition across the array (Methods). On the basis of spatial patterns of pollutant deposition, state-of-the-art FLEXPART atmospheric aerosol transport and deposition modelling (Methods), historical information including regional commodity production statistics, and Pb isotopic measurements, we determined the likely dominant emission source and evaluated the extent and severity of consequent air pollution. We assessed potential impacts of these As and Pb emissions on late nineteenth- and early twentieth-century human health using findings from modern epidemiology studies and census data (Methods).

Results

The Summit2023 record measured at high resolution using the continuous analytical system shows that pre-Industrial Revolution background levels of As were low, but well above concentrations expected from crustal dust alone indicated by an average enrichment (enrAs) of 14 between 1850 and 1869 (Fig. 1). Enrichments rose slowly to ~45 by 1887, rapidly from 1888 to ~1895 to ~150, and then more slowly until World War I (WWI) when enrAs reached >200 or 15 times pre-Industrial Revolution background levels. Enrichments declined rapidly following WWI to ~40 in 1920, recovered to >65, and then dropped again to 1850–1869 background levels during the 1932–1934 nadir of the Great Depression. While enrichments increased again after the Depression, they remained well below 1898–1918 levels through 1950 and more generally through 2020. Changes in As and ncAs (Fig. 1) concentrations and depositional fluxes were similar, with ncAs deposition fluxes increasing from a pre-Industrial Revolution background of ~0.8–7.4 μg m^{-2} yr^{-1} between 1914 and 1918. Following the end of WWI, ncAs fluxes declined sharply to

https://doi.org/10.1038/s41893-026-01975-9

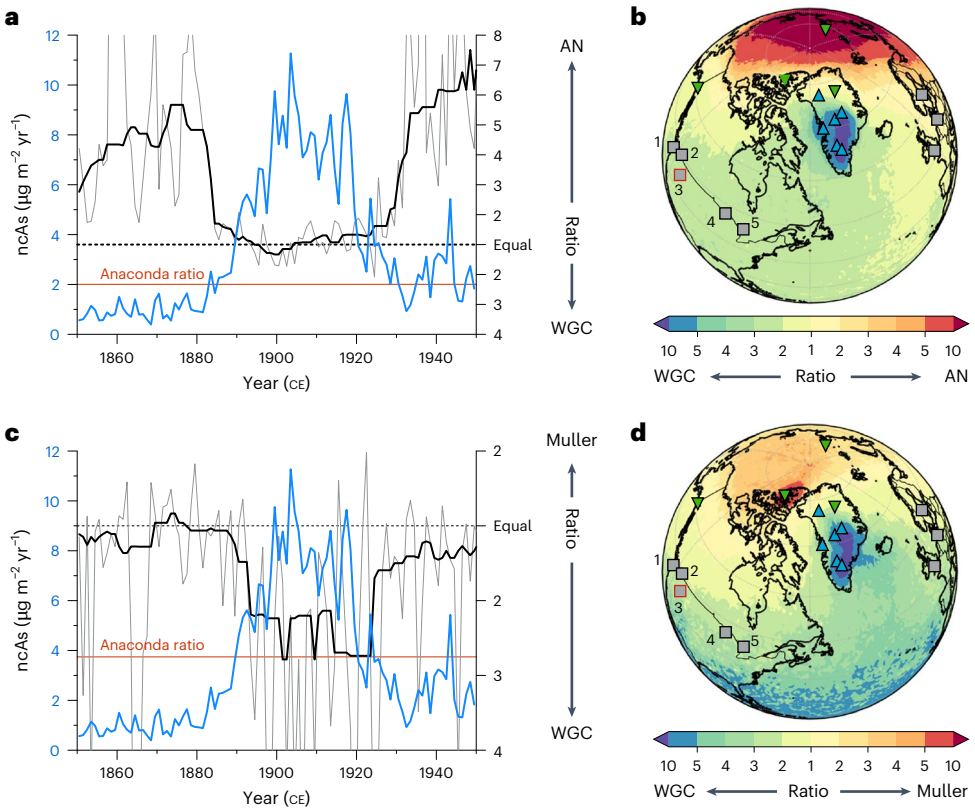


Fig. 2 | Relative arsenic deposition in Greenland and the Canadian and Russian Arctic. a, 1850–1950 annual ncAs flux measured in Summit2023 and the annual (light) and 11-yr median-filtered (dark) Russian Arctic AN to Greenland WGC ncBi flux ratio (as a proxy of ncAs). **b**, AN to WGC ratio in FLEXPART-simulated emission sensitivities, with triangles showing ice core locations and squares showing major pre-WWI base-metal mining and smelter complexes (northern NA: 1 – Tacoma, 2 – Trail, 3 – Butte/Anaconda, 4 – Keweenaw, 5 – Sudbury). **c**,**d**, Same as **a** and **b** but for Muller2025-SC. Ratios at both ice core sites during the late nineteenth and early twentieth century ncAs anomaly in Greenland show proportionally larger fluxes in Greenland (that is, WGC) consistent with northern NA smelter emissions. Northern Eurasian emissions would have resulted in proportionally greater fluxes in the Russian Arctic and Arctic Canada.

~3.4 μg m^{-2} yr^{-1} between 1919 and 1929 and then to ~1.0 during the Great Depression, only slightly above the 1850–1869 background. Annual ncAs fluxes remained well below early twentieth century deposition rates through 2020, generally between 1 and 3 μg m^{-2} yr^{-1}. Enrichments, concentrations and fluxes of total and non-crustal Bi (ncBi versus ncAs, $r > 0.94$, $n = 58$, $P << 0.0001$) and Sb (ncSb versus ncAs, $r = 0.93$, $n = 58$, $P << 0.0001$) in Summit2023 varied similarly to ncAs between 1875 and 1932, suggesting common sources (all P values reported in this study are single sided). Moreover, ncAs concentrations closely tracked ncBi and with a consistent concentration ratio in Summit2023 and in the three other cores in which As was measured (Extended Data Fig. 1), implying that ncBi can be used as a proxy of ncAs during this period.

Non-crustal Pb measured in the Summit2023 ice core also showed strong similarities to ncAs between 1850 and 1950 but with some important differences (Extended Data Fig. 2). Consistent with earlier studies[2,25], enrichment (enrPb) averaged ~30 and was relatively constant during the pre-Industrial Revolution background period but increased to ~60 by 1880 and >130 by 1885. enrPb remained high but variable until the end of WWI before declining sharply to ~60 immediately following WWI and then nearly to 1850–1869 background levels during the Depression, before increasing again to >250 in the late 1960s. The initial rise in enrPb from 1870 to 1880 indicates emission sources that did not contain appreciable amounts of As, Bi or Sb, and Pb isotopic ratios measured in the Summit2023 and Tunu2022b cores during this period are consistent with a mixture of western European and North American coals. However, 1880 to 1932 annual variations in enrPb and enrAs were similar ($r = 0.76$, $n = 53$, $P << 0.0001$) and even more similar between 1898 and 1918 ($r = 0.88$, $n = 21$, $P << 0.0001$), suggesting that some sources were common to both metals especially during the latter period. ncPb fluxes followed a similar pattern, increasing from a pre-Industrial Revolution background average of 4.1 to an average of 15.4 μg m^{-2} yr^{-1} between 1898 and 1918 and 16.3 μg m^{-2} yr^{-1} between 1914 and 1918 during WWI, before declining to ~8.0 μg m^{-2} yr^{-1} between 1930 and 1934 during the Depression but still well above 1850–1869 background.

Year-to-year variations in meteorology and long-range atmospheric transport, in addition to glaciological noise from small-scale spatial variability in the timing of snow accumulation, result in uncertainties in a single ice core record of aerosol deposition[2,24,29]. Because of highly significant correlations between the ice core pollutant records from western Greenland (Extended Data Table 2), we developed multicore, western Greenland composites (WGC) of ncBi, ncSb and ncPb (Fig. 1) using the geometric means (that is, log averages) of the six records (five for ncSb because we did not measure Sb in NUUS2015; Extended Data Figs. 3 and 4). We also developed a WGC emission sensitivity field using the geometric mean of the six individual FLEXPART emission sensitivity fields to underpin interpretation.

Discussion

Source attribution

Continuous As measurements in three widely spaced cores and discrete As measurements in Logan2022 (Extended Data Fig. 1) all showed similar 1875–1932 ncAs/ncBi ratios (26.7 ± 0.8 1 s.e., $P < 0.0001$ and 26.4 ± 1.8 1 s.e., $P < 0.0001$ for the continuous and discrete measurements, respectively). Together with the highly significant ($P < 0.0001$) co-variability in the WGC pollutant records (Extended Data Table 2 and Fig. 3), this suggests that common emission sources influenced western Greenland during the pronounced high concentration anomaly

https://doi.org/10.1038/s41893-026-01975-9

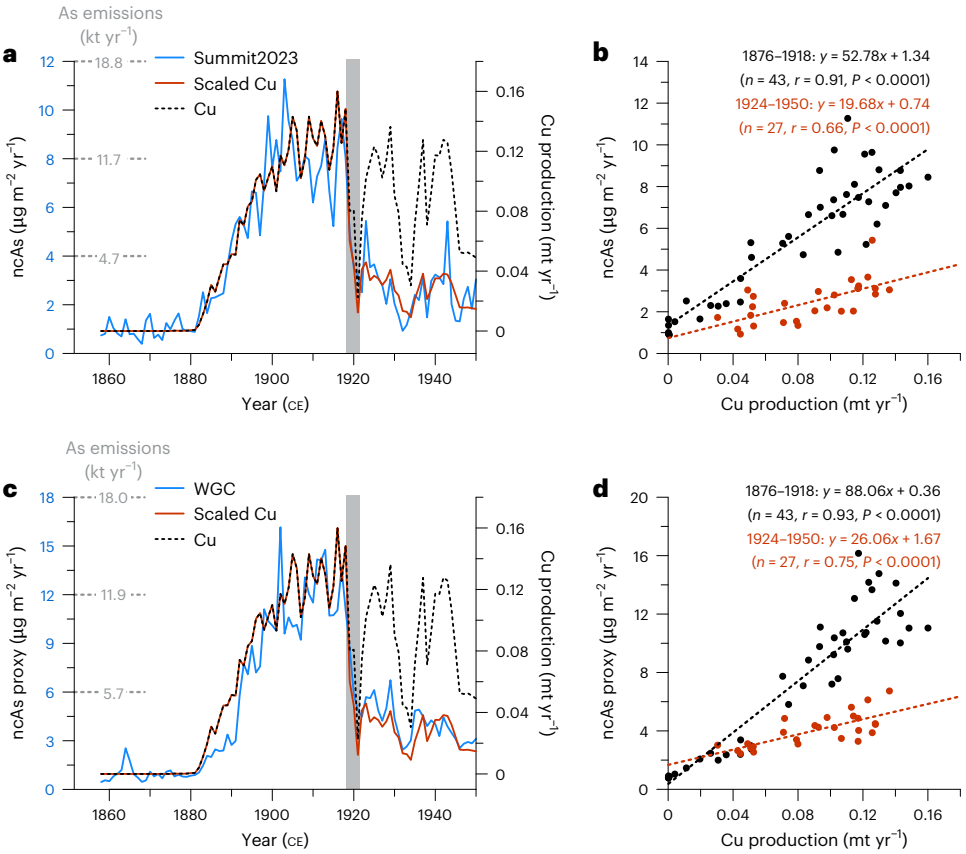


Fig. 3 | Comparison between annual Montana Cu production and As pollution in Greenland before and after pollution abatement. a, ncAs deposition in Summit2023 (blue) before and after phased ~1919–1923 (grey bar) installation of Cottrell electrostatic precipitators (EP) at the Washoe (Butte/Anaconda) smelter. Arsenic emissions are based on observed fluxes divided by the FLEXPART-simulated emission sensitivity and compare well to emissions of 5.6–15.7 kt yr^{-1} estimated from spot measurements of the exhaust fumes before 1919. **b**, Evaluations before (black) and after (red) EP installation indicate ~65% reduction in relative ncAs emissions. For illustration, Montana Cu production is shown in **a**, after scaling (red) to reflect this reduction (scaler, 1 from 1850 to 1918; 0.35 from 1924 to 1950). **c**,**d**, Same as **a** and **b** but for ncAs proxy flux based on ncBi measured in the WGC array. Pearson's *r* probabilities are one sided.

particularly for ncAs and ncBi, but also for substantial portions of ncSb and ncPb fallout especially after ~1895. Pollutant deposition generally decreases with distance from the source. Thus, comparing ncAs and ncBi deposition in different ice cores may provide information on the location of the source. Following an approach previously used to interpret broad arrays of Arctic and Antarctic ice core aerosol records[2,11,20], we evaluated ratios of annual ncBi deposition (as a proxy of ncAs) in ice cores from other parts of the Arctic relative to WGC against similar ratios in their respective FLEXPART emission sensitivity fields (Fig. 2). While the absolute magnitude may be biased by different background fluxes, changes in the deposition ratios can indicate the location of the additional emission sources, provided there are sufficient differences between the two airsheds (that is, the geographic region from which atmospheric aerosol emissions influence impurity deposition at an ice core site[21]). Comparisons of ncBi fluxes in WGC against (1) Muller (Muller2025-SC) from far northern Canada and (2) Akademii Nauk (AN) from the Russian Arctic both show clear and sustained shifts in the deposition ratios towards WGC during the pronounced ~1888–1918 ncAs anomaly in Greenland. The emission sensitivity ratio maps show that only emissions from northern NA are consistent with these marked changes. That is, northern NA shows high WGC ratios, indicating that additional emissions from these regions enhance deposition in western Greenland relative to other sites.

Cu smelters are thought to be among the largest sources of current As pollution[7] and demand for Cu and other base metals increased rapidly in the late nineteenth and early twentieth centuries following widespread electrification and development of myriad industrial and military uses during the buildup to WWI[30]. While the pollutant deposition patterns (Fig. 2) clearly implicate emissions from northern NA, relatively few large-scale, non-ferrous mining and smelting sites were in operation in this region before WWI (Methods). The largest were located on Michigan's Keweenaw Peninsula and near Butte/Anaconda in western Montana. Most of the production on the Keweenaw Peninsula, however, was from native Cu[31] so As, Bi, Sb and Pb emissions were relatively low. Moreover, production in the Keweenaw Peninsula started decades before the anomalies recorded in Greenland ice (Extended Data Fig. 5).

Cu production in Montana which started in the 1870s was almost entirely from sulfide ores mined near Butte, and most of the ores were processed locally or in nearby Anaconda and Great Falls as early as 1884 but especially after construction of the enormous Washoe smelter in Anaconda in 1902 and consolidation of mine and smelter ownership[31,32]. Massive emissions from roasting and smelting of these sulfide ores were well-known sources of sulfuric acid and volatile heavy metal emissions at the time (for example, As, Bi, Sb, Pb, Hg). Damages from As emissions resulted in decades of litigation between the operators of Butte/Anaconda and nearby ranchers, farmers and eventually the US Forest Service[31,32]; the Silver Bow Creek/Butte Area Superfund site is now among the largest and most toxic environmental remediation sites in the United States[31]. Butte/Anaconda was the world's largest Cu producer from 1892 to 1903 and production dwarfed that at other northern NA sites except Keweenaw well into the twentieth century (Extended Data Fig. 5). Highly significant correlations between 1876 and 1918 annual Montana Cu production (for example,

https://doi.org/10.1038/s41893-026-01975-9

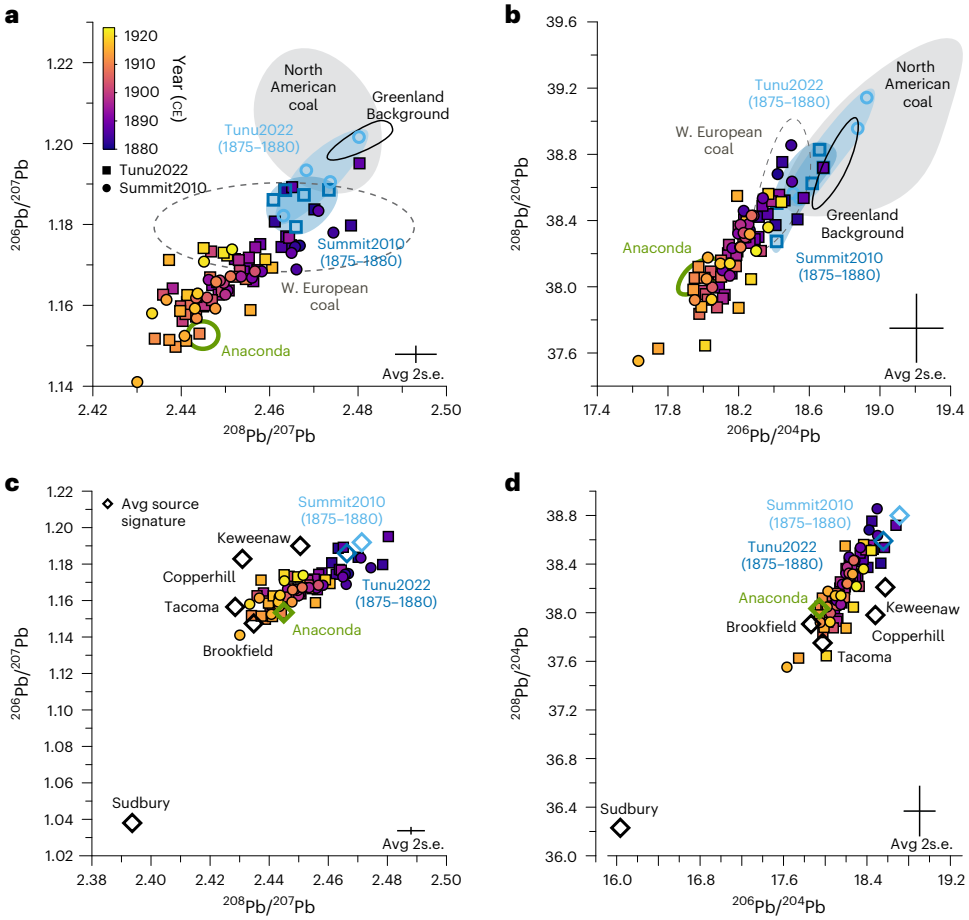


Fig. 4 | Three-isotope plots of 1880–1920 Pb isotopic measurements in the Summit2023 and Tunu2022b ice cores with selected potential pre-WWI emission sources. a,**c**, ^{206}Pb, ^{207}Pb, ^{208}Pb. **b**,**d**, ^{204}Pb, ^{206}Pb, ^{208}Pb. Background 1875–1880 ratios at both core sites before substantial emissions from most northern NA Cu production sites are consistent with a mixture of Western European and North American coals. The isotopic ratios measured in the ice generally fall on a mixing line between the coal background and ore bodies and/or smelting of Cu at Butte/Anaconda MT, Tacoma WA and Sudbury ON, and gold at Brookfield NS, although operations at Butte/Anaconda were orders of magnitude greater than at the other locations during this period. The isotopic ratios in the ice are not consistent with fallout dominated by emissions from Cu mining and smelting at Keweenaw MI, Copperhill TN or Sudbury ON.

ref. 33) and ncAs fluxes measured in the Summit2023 core ($r = 0.90$, $n = 44$, $P << 0.0001$), as well as ncBi ($r = 0.93$, $n = 44$, $P << 0.0001$) and ncSb ($r = 0.86$, $P << 0.0001$) fluxes measured in the WGC array, suggest Butte/Anaconda emissions as the primary source of As, Bi and Sb pollution in western Greenland during this period (Fig. 3). In addition, the ncAs/ncBi ratio of 26.6 (±0.5 s.e.) in Greenland pollution (Extended Data Fig. 1) is nearly identical to the ratio of 25.2 (uncertainties not available) estimated from 1911 spot measurements of Anaconda smelter exhaust fumes[34]. Similar comparisons between Greenland pollution and regional Cu and base-metal production from other potential northern NA sources showed no significant co-variation (Extended Data Fig. 5).

Following an approach employed in previous interpretations of arrays of ice core records using backward FLEXPART aerosol modelling[16,20], we estimated year-by-year (Fig. 3) and average emissions from Butte/Anaconda based on deposition measured in the WGC array. This approach yielded average emissions of 30 t d^{-1} or 11 kt yr^{-1} for As during the 1898–1918 period of maximum As pollution (Fig. 1). These rates are similar to estimates from spot measurements of As in the Washoe smelter exhaust fumes during this period, ranging from 5.8 to 15.7 kt yr^{-1} (ref. 31). For perspective, it is estimated that Chilean Cu smelters which are among the largest modern sources of atmospheric As emissions cumulatively released ~3 kt of As in 2015[5].

While several lines of evidence suggest that emissions from Butte/Anaconda Cu production were the dominant sources of As, Bi and Sb pollution in western Greenland, multiple sources (for example, fossil-fuel combustion) and source regions probably contributed to ncPb pollution during this period. Spot measurements of As and Pb in the Washoe smelter exhaust fumes and dust in 1911 indicated Pb/As emission ratios of 0.4 (ref. 34), resulting in estimated 1898–1918 average Pb emissions of 4.4 kt yr^{-1} that would account for ~20% of the non-crustal Pb deposited in the WGC array during this period. To further investigate this, we used new and existing Pb isotopic measurements in the Tunu2022b and Summit2010[9] ice cores, respectively, as well as the Bayesian isotopic mixing model MixSIAR (Methods) and potential source signatures to estimate Butte/Anaconda Pb emissions. The Summit2010 and Summit2023 cores were drilled near each other and annual average Pb concentrations measured from 1875 to 1932 in the two cores are highly correlated ($r > 0.96$, $n = 58$, $P << 0.0001$). Background Pb isotopic ratios from 1875 to 1880 before the start of substantial Butte/Anaconda (and other northern NA) base-metal mining and smelting other than on the Keweenaw Peninsula, were similar in both Summit2010 and Tunu2022b (Fig. 4), and consistent with a mixture of emissions from western European and North American coal combustion. The 1880–1920 isotopic ratios measured in the ice generally fall on a mixing line between the coal background and ore bodies and/or smelting emissions at

https://doi.org/10.1038/s41893-026-01975-9

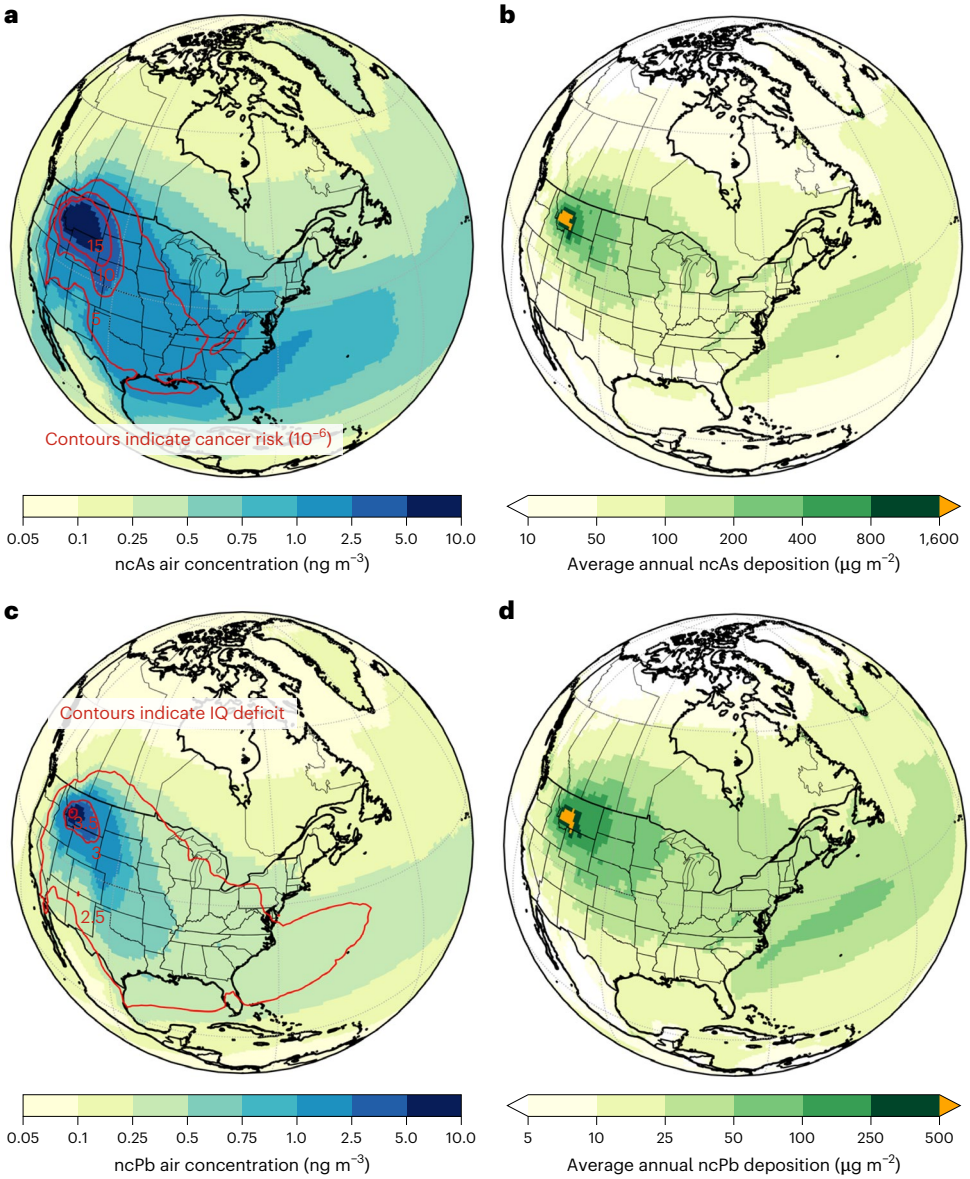


Fig. 5 | Estimated air pollution concentrations, deposition and potential health impacts from Montana copper production. FLEXPART-simulated, non-background (nb) **a**,**b**, air pollution concentrations and **c**,**d**, fluxes of As and Pb resulting from estimated average 1898–1918 emissions of 11 and 4.4 kt yr^{-1} from Butte/Anaconda, respectively. Contours show estimated **a**, EPA-based cancer risk for arsenic and **c**, IQ deficits for lead exposures.

Butte/Anaconda MT, Tacoma WA, Sudbury ON and Brookfield NS. Although similarities in the isotopic ratios preclude more specific attribution, operations at Butte/Anaconda were orders of magnitude greater than at the other locations. Pb contributions predominately from Sudbury ON, the Keweenaw Peninsula MI and Copperhill TN are not consistent with the isotopic ratios in the ice (Fig.4). MixSIAR source apportionment in Tunu2022b and Summit2023 (Fig. 4) that accounts for uncertainties (Methods) suggests 1898–1918 average Butte/Anaconda emissions of ~7 ± 4 and ~14 ± 5 kt yr^{-1}, respectively, accounting for ~60% of Pb pollution at both sites during this period. However, even minor inputs of Pb from sources not included in the MixSIAR modelling could have substantially altered the observed average Pb isotopic ratios, resulting in an overestimate of Butte/Anaconda Pb emissions (Fig. 4). Therefore, we used the more conservative ~4.4 kt yr^{-1} (uncertainties not available) implied by the estimated As emissions and contemporaneous Pb/As spot measurements of the exhaust[31,34] to evaluate atmospheric Pb concentrations and potential health implications.

Pollution abatement

Pollution abatement efforts eventually implemented at Butte/Anaconda principally involved the phased ~1919–1923 installation of Cottrell electrostatic precipitators at the Washoe smelter[35] intended to recover valuable Cu and As from the exhaust fumes[31]. Although less closely than during the 1876–1918 period before precipitator installation, annual 1924–1950 Montana Cu production also covaried with Summit2023 ncAs ($r = 0.66$, $n = 26$, $P << 0.0001$) and WGC ncBi ($r = 0.75$, $n = 26$, $P << 0.0001$) deposition, suggesting that emissions from Butte/Anaconda Cu production remained the dominant source of ncAs and ncBi pollution in Greenland at least until 1950. Comparisons of 1924–1950 annual ncSb and ncPb fluxes in the WGC array with Montana Cu production showed little covariance indicating important additional sources of these two pollutants. Assuming Butte/Anaconda remained the dominant source and no other changes in smelter operations, the efficacy of Cottrell electrostatic precipitators in reducing emissions is estimated to be 63% for As and 70% for Bi (Fig. 3), meaning 53.0 (±3.8 s.e.) and 19.7 (±4.5 s.e.) µg m^{-2} of ncAs pollution were deposited

at Summit for every megatonne (mt) of Cu produced at Butte/Anaconda before and after precipitator installation, respectively. These estimates are somewhat lower than the 80–90% efficacy for As reported by Anaconda smelter staff in 1923/24 on the basis of spot exhaust fume measurements[31,36], but nearly identical to estimates of ~67% based on other contemporaneous exhaust fume measurements[32,35]. Although substantially reduced by the precipitator installation, As and other toxic emissions from Butte/Anaconda were still large after 1923.

Health implications

Emissions from Butte/Anaconda resulted in dangerous air concentrations over large parts of North America exemplified by pollution deposition across the WGC ice core array located 4,200 to 4,700 km from Butte/Anaconda (Extended Data Table 1) and potentially led to widespread health impacts (Fig. 5). On the basis of the 1910 and 1911 census records from the United States and Canada, respectively, forward FLEXPART modelling, and 1898–1918 average As emissions of 11 kt yr^{-1}, we estimate that 55% of Americans (50.5 million) and ~11% of Canadians (0.6 million) were exposed to average air concentrations >1 ng m^{-3}. According to modern epidemiology findings, this exposure corresponded to elevated lifetime risk for lung cancer ($1.5/10^6$ to $5/10^6$) as well as other serious ailments (Methods). Moreover, ~0.5% of Americans (0.43 million), including 93%, 28% and 13% of Montana, Wyoming and Idaho residents, respectively, were exposed for nearly 30 years to As concentrations >6 ng m^{-3}. This is the current maximum threshold level for chronic exposure recommended by the World Health Organization (WHO), corresponding to elevated lifetime risk for lung cancer of $10/10^6$ to $30/10^6$. For perspective, recent background As air concentrations in Europe and the United States typically range from 0.1 to 0.5 ng m^{-3} (ref. 5). Similar evaluation of Pb concentrations in air using a conservative Pb emission rate of 4.4 kt yr^{-1} during this period (<7–14 kt yr^{-1} estimated from the lead isotopic records but consistent with the Pb/As ratio measured in the smelter exhaust fumes) indicates that 1.4 million Americans and Canadians, including all residents of Montana and Wyoming, were exposed to air pollution concentrations elevated by >1 ng m^{-3}, while >0.27 million were exposed to >5 ng m^{-3}, including 74% of Montanans. Although it is difficult to estimate cognitive impacts without knowing ambient concentrations and background exposures, a >1 ng m^{-3} increase would have enhanced blood lead levels (BLLs) by >2.6 μg dl^{-1} in especially vulnerable children under 5 years, leading to widespread cognitive decline equivalent to IQ reductions of >2.6 points assuming preexisting BLLs of 1 μg dl^{-1}. Here we focused on potential health effects from inhalation of primary As and Pb emissions, and not any additional impacts of increased heavy metal deposition over soils, crops and water supplies or resuspension of deposited heavy metals. We emphasize that current epidemiological understanding is that no level of exposure to As or Pb is without risk.

Lax regulation and delayed emission reductions

The Cottrell electrostatic precipitator was patented in 1908, and precipitators were soon widely adopted by smelters in the western United States and Canada (for example, the Trail BC smelter in 1914[37]) as an effective means for removing sulfur (S), As, Pb and other toxic heavy metals from ore processing emissions. Cottrell was contracted by the Anaconda Smoke Commission in 1913 to investigate ways to reduce emissions by enhancing recovery of valuable Cu, S and As from the exhaust fumes[31,35]. Final installation of electrostatic precipitators at Butte/Anaconda, which our findings suggest reduced heavy metal emissions by ~65% (Fig. 3), however, was delayed for nearly a decade until 1923. This delay was partly because of technological challenges associated with the scale of the emissions but mainly because of regulatory policy at the time that required installation of emissions controls only if profitable to the polluter[31,35]. We estimate that this delay resulted in additional atmospheric As and Pb releases of ~60 and ~24 kt, respectively, unnecessarily exposing hundreds of thousands or millions of Americans and Canadians to dangerously elevated toxic heavy metal air concentrations for many years, while depositing additional kilotons of these toxins over much of North America, including over Greenland nearly a continent away.

Methods

Ice core records

The ice cores were collected using electro-mechanical drills and handled in the field following standard procedures. Details can be found in the citations listed for each core in Extended Data Table 1. All cores were analysed for a broad range of elements and chemical species using the well-established continuous ice core analytical system at the Desert Research Institute (DRI)[27,28]. Included were S, sodium (Na) and calcium (Ca) that underpinned volcanically constrained annual layer counting used to establish ice core chronologies[2], cerium (Ce) used here as a crustal dust indicator, and potential heavy metal and metalloid pollution such as Bi, Sb and Pb. Typical detection limits defined as three times the standard deviation of the blank were 0.0009, 0.0005, 0.0004 and 0.0001 ng g^{-1} for Ce, Sb, Pb and Bi, respectively. Following ref. 11, non-crustal concentrations and enrichments were derived from measured total concentrations using simultaneous measurements of the rock-forming rare earth element Ce and relative mean soil abundances for Ce (83 μg g^{-1}) and each metal (As 7.7 μg g^{-1}, Bi 0.4 μg g^{-1}, Sb 1.2 μg g^{-1}, Pb 19 μg g^{-1})[38]. Annual depositional fluxes were calculated as the product of the annual average concentration and the recent average net water-equivalent snow accumulation rate at each site (Extended Data Table 1) following standard procedures.

Arsenic measurements

The DRI continuous method was expanded in 2024 to include As, so concentrations of arsenic were measured continuously in the Tunu2022b, Summit23 and Muller2025-SC ice cores. The DRI analytical system includes two Thermo Element2 high-resolution inductively couple mass spectrometers (HR-ICP-MS) operating in parallel to make simultaneous measurements of a broad range of elements. Because of possible isobaric interferences, As is ideally measured in high HR-ICP-MS slit resolution, resulting in relatively low sensitivity. However, extensive comparisons of As measured discretely and continuously in low, medium and high slit resolutions in Summit2023 (Extended Data Fig. 6), Tunu2022b, Muller2025-SC and Logan2022 ice samples suggest that isobaric interferences are minimal when analysing meltwater at these sites. Therefore, continuous analyses conducted in low-resolution were used in the interpretation to maximize sensitivity. During the Tunu2022b analysis, typical As detection limits for low slit resolution were 0.0003 ng g^{-1}. This compares to typical annual average As concentrations of ~0.0022 ng g^{-1} and monthly As concentrations ranging from ~0.0007 to ~0.005 ng g^{-1} in pre-industrial ice. Until the early twenty-first century, As concentrations during much of the industrial period were an order of magnitude (or more) higher. Discrete measurements of As, Bi and Ce in the Logan2022 core were made on discrete acidified samples of meltwater that had been collected during the continuous analyses in ice corresponding to 1873–1999.

Determining proxy ncAs records from measured ncBi

Annual concentrations of ncAs closely tracked ncBi (Extended Data Fig. 1) from 1850 to 1950 in each of the three ice cores with continuous As and Bi measurements. The ncAs/ncBi ratios during the 1875–1932 period of focus were 26.1 (±0.61 s.e., $r = 0.98$, $n = 58$, $P << 0.0001$) and 27.4 (±0.88 s.e., $r = 0.97$, $n = 58$, $P << 0.0001$) in the two Greenland records (Summit2023, Tunu2022b) and 30.7 (±0.94 s.e., $r = 0.97$, $n = 58$, $P << 0.0001$) in the Muller2025-SC core from northeastern Canada. Concentrations of ncAs and ncBi from 1877 to 1931 also covaried in the discrete Logan2022 measurements ($r = 0.96$, $n = 21$, $P < 0.0001$), with an ncAs/ncBi ratio of 26.4 (±1.8 s.e.). As a result, we created proxy ncAs records from the measured ncBi concentrations in the five cores

in the WGC array that did not have As measurements using an ncAs/ncBi scaler of 27.

Atmospheric aerosol deposition and transport modelling

The state-of-the-art atmospheric aerosol transport and deposition model FLEXPART[39] was used in backward mode to determine emission sensitivity fields[40] at all of the ice core sites (Extended Data Table 1). Without detailed meteorological fields necessary for such modelling throughout the 1850–2020 study period, we assumed as in previous studies[2,11,16,20,24] that meteorological conditions driving large-scale atmospheric transport were relatively stable. Therefore, 1960–1969 backward FLEXPART (v.11)[41] simulations were conducted using global ERA-5 reanalysis data (0.5° × 0.5° resolution, 137 vertical layers, of which 41 are located below 5,000 m asl[42]). Furthermore, we assumed that metallurgical processes emitted heavy metals in the gaseous phase that quickly adsorbed onto ambient 1 µm dust particles, and these relatively inert small particles were transported to higher latitudes and deposited in glaciers and ice sheets (for example, ref. 24). To test sensitivity to the assumed ambient aerosol type, we also performed separate calculations for 5 µm mineral dust, as well as sulfate and black carbon aerosols with assumed diameters of 0.4 µm (refs. 2,24). Using atmospheric As emissions from Butte/Anaconda constrained by the ice core heavy metal records and backward FLEXPART simulations, we estimated atmospheric As concentrations and depositional fluxes across the Northern Hemisphere on the basis of forward FLEXPART simulations.

Lead isotopic ratios

We used previously published Pb isotopic ratios from the nearby Summit2010 core[9] because such measurements were not made on the Summit2023 core. For Tunu2022b and Logan2022 (Extended Data Table 1), Pb isotopic ratios were measured following established methods[9,11] in meltwater samples routinely collected as part of the continuous ice core measurements[24]. Briefly, reconstituted acidified samples were introduced into an Element2 HR-ICP-MS (Thermo) using an Apex IR inlet system fitted with a PFA MicroFlow nebulizer (Elemental Scientific) and N_2 used as the additional gas.

All samples and standards were normalized to the bracketing standard (National Institute of Standards and Technologies (NIST, USA) SRM 981 natural lead (isotopic) standard). Procedural blanks for the Tunu2022 and MountLogan2022 ice cores contributed an average of 0.6 ± 0.3% and 0.2 ± 0.1% of the sample lead signal, respectively. Measured reference materials differed from published values for BCR-2 Columbia River Basalt[43] and AGV-1 Guano Valley Andesite, and NIST 1643f Trace Elements in Water[9] by 0.5% for $^{206}Pb/^{207}Pb$ and 0.3% for $^{208}Pb/^{207}Pb$.

We used the Bayesian isotopic mixing model MixSIAR (v.3.1.12)[44] to apportion sources of late nineteenth- to early twentieth-century Pb pollution in Greenland and Canada based on the Tunu2022, Summit2010 and MountLogan2022 measurements. MixSIAR was chosen over a simple linear mixing model because it accounts for source heterogeneity[44] and has been successfully applied to the stable Pb isotopic system[11,45]. The end-member isotopic compositions were defined using coal sources from North America[46,47] and Western Europe[47–49], as well as smelting sources that most likely contributed to emissions from Anaconda[50,51] and Sudbury[52–54]. Other sources[55–59] were considered, but either did not appreciably contribute to the MixSIAR results or were removed due to the timing of their use.

Non-ferrous mining and smelting in northern North America

The pollutant deposition patterns in the Arctic and near-Arctic (Fig. 2) point to emissions from northern NA. However, only a few large-scale non-ferrous mining and smelting sites were in operation in these higher-latitude regions before and during WWI. These included Butte/Anaconda MT (46.1° N, 112.9° W), the Keweenaw Peninsula MI (47.1° N, 88.6° W) and a Pb/Cu smelter in Tacoma WA (47.3° N, 122.5° W)[60] in the United States, as well as Canadian complexes near Sudbury ON (46.5° N, 48.2° W), Trail BC (49.1° N, 117.8° W) and smaller operations such those near Ely QC[30], although by far the largest two before and during WWI were Butte/Anaconda and on Keweenaw Peninsula. For example, although the Canadian Horne smelter located at Rouyn-Noranda (48.3° N, 79.0° W) and the Flin Flon (54.8° N, 101.9° W) mine and associated ore processing activities were well-documented sources of atmospheric As emissions[61], operations did not start until the mid to late 1920s, while activities at another major source of high-latitude arsenic emissions, the Canadian Giant Mine (62.5° N, 114.4° W), only started in the late 1940s[30].

Effects of As and Pb exposure on human health

Although current understanding is that no level of As or Pb exposure is free of risk and exposure has been linked to a range of ailments including lung, bladder, liver and other cancer, diabetes, cognitive decline and heart disease, here we focus on lung cancer risk (CR) from chronic background As exposure and cognitive decline for Pb exposure. To estimate CR (10^{-6}), we multiplied FLEXPART-simulated 1988–1918 average air concentrations (µg m^{-3}) by the EPA Inhalation Unit Risk of 0.0043 µg m^{-3} (ref. 62), although we acknowledge that the WHO Inhalation Unit Risk is about a factor of three lower[63]. To estimate health impacts of enhanced Pb exposure from the conservative average 1898–1918 Butte/Anaconda emissions of 4.4 kt yr^{-1}, we followed the approach of ref. 16. Literature-based, modern nonlinear relationships between (1) ambient concentrations of Pb in air and BLLs for different age groups were used to estimate BLL enhancements, and (2) linkages between BLL and IQ deficit[8,64] were used to assess possible levels of additional cognitive decline assuming a background BLL of 1 µg dl^{-1}. For BLL enhancements, we used the log-linear model BLL (µg dl^{-1}) = exp(1.932(±0.181) + 0.140(±0.054) × ln(air concentration)) for 1–5-year-old children[65]. IQ deficits associated with these BLLs were estimated using a log-linear model with IQ deficit = −3.315(±0.6155) × ln(BLL + 1)[64]. For both models, reported uncertainties are 1 s.d.

Reporting summary

Further information on research design is available in the Nature Portfolio Reporting Summary linked to this article.

Data availability

Data that underpin the findings of this study are available in figshare at https://doi.org/10.6084/m9.figshare.33991051 (ref. 66).

Code availability

The FLEXPART and MixSIAR models used in this study are available at https://www.flexpart.eu/ (ref. 67) and https://github.com/brianstock/mixsiar (ref. 68), respectively. All maps were created using Python's Cartopy (v.0.11.2.22-Aug-2014 Met Office, UK) and Natural Earth's public domain vector data. Cartopy is available at https://github.com/SciTools/cartopy/archive/v0.11.2.tar.gz.

References

1. McConnell, J. R. & Edwards, R. Coal burning leaves toxic heavy metal legacy in the Arctic. *Proc. Natl Acad. Sci. USA* **105**, 12140–12144 https://doi.org/10.3109/10408444.2013.832726 (2008).
2. McConnell, J. R. et al. Pervasive Arctic lead pollution suggests substantial growth in medieval silver production modulated by plague, climate, and conflict. *Proc. Natl Acad. Sci. USA* **116**, 14910–14915 https://doi.org/10.1073/pnas.1904515116 (2019).
3. Lee, K. et al. A 300-year high-resolution Greenland ice record of large-scale atmospheric pollution by arsenic in the Northern Hemisphere. *Environ. Sci. Technol.* **53**, 12999–13008 https://doi.org/10.1021/acs.est.9b01805 (2019).
4. World Health Organization. *Human Health Effects of Benzene, Arsenic, Cadmium, Nickel, Lead and Mercury: Report of an Expert Consultation* (WHO, 2024).

5. Zhang, L. et al. Global impact of atmospheric arsenic on health risk: 2005 to 2015. *Proc. Natl Acad. Sci. USA* **117**, 13975–13982 https://doi.org/10.1073/pnas.2002580117 (2020).
6. Mohammed Abdul, K. S., Jayasinghe, S. S., Chandana, E. P. S., Jayasumana, C. & De Silva, P. M. C. S. Arsenic and human health effects: a review. *Environ. Toxicol. Pharmacol.* **40**, 828–846 https://doi.org/10.1016/j.etap.2015.09.016 (2015).
7. Schlesinger, W. H., Klein, E. M. & Vengosh, A. The global biogeochemical cycle of arsenic. *Global Biogeochem. Cycles* **36**, e2022GB007515 https://doi.org/10.1029/2022GB007515 (2022).
8. Lanphear, B. et al. Low-level environmental lead exposure and children's intellectual function: an international pooled analysis. *Environ. Health Perspect.* **113**, 894–899 https://doi.org/10.1289/ehp.7688 (2005).
9. Wensman, S. M., Shiel, A. E. & McConnell, J. R. Lead isotopic fingerprinting of 250-years of industrial era pollution in Greenland ice. *Anthropocene* **38**, 100340 https://doi.org/10.1016/j.ancene.2022.100340 (2022).
10. Gabrielli, P. et al. Early atmospheric contamination on the top of the Himalayas since the onset of the European Industrial Revolution. *Proc. Natl Acad. Sci. USA* **117**, 3967–3973 https://doi.org/10.1073/pnas.1910485117 (2020).
11. McConnell, J. R. et al. Hemispheric-scale heavy metal pollution from South American and Australian mining and metallurgy during the Common Era. *Sci. Total Environ.* **912**, 169431 https://doi.org/10.1016/j.scitotenv.2023.169431 (2024).
12. Rosman, K., Chisholm, W., Hong, S., Candelone, J. & Boutron, C. Lead from Carthaginian and Roman Spanish mines isotopically identified in Greenland ice dated from 600 BC to 300 AD. *Environ. Sci. Technol.* **31**, 3413–3416 https://doi.org/10.1021/es970038k (1997).
13. Wolff, E. W. & Suttie, E. D. Antarctic snow record of Southern-Hemisphere lead pollution. *Geophys. Res. Lett.* **21**, 781–784 https://doi.org/10.1029/94GL00656 (1994).
14. Gross, B. H. et al. Constraining recent lead pollution sources in the North Pacific using ice core stable lead isotopes. *J. Geophys. Res.* **117**, D16307 https://doi.org/10.1029/2011JD017270 (2012).
15. Murozumi, M., Chow, T. J. & Patterson, C. Chemical concentrations of pollutant lead aerosols, terrestrial dusts and sea salts in Greenland and Antarctic snow strata. *Geochim. Cosmochim. Acta* **33**, 1247–1294 https://doi.org/10.1016/0016-7037(69)90045-3 (1969).
16. McConnell, J. R. et al. Pan-European atmospheric lead pollution, enhanced blood lead levels, and cognitive decline from Roman-era mining and smelting. *Proc. Natl Acad. Sci. USA* **122**, e2419630121 https://doi.org/10.1073/pnas.2419630121 (2025).
17. McConnell, J. R. et al. Antarctic-wide array of high-resolution ice core records reveals pervasive lead pollution began in 1889 and persists today. *Sci. Rep.* **4**, 5848 https://doi.org/10.1038/srep05848 (2014).
18. Moseid, K. O. et al. Using ice cores to evaluate CMIP6 aerosol concentrations over the historical era. *J. Geophys. Res.* **127**, e2021JD036105 https://doi.org/10.1029/2021JD036105 (2022).
19. McConnell, J. R. New directions: historical black carbon and other ice core aerosol records in the Arctic for GCM evaluation. *Atmos. Environ.* **44**, 2665–2666 https://doi.org/10.1016/j.atmosenv.2010.04.004 (2010).
20. McConnell, J. R. et al. Hemispheric black carbon increase after the 13th-century Māori arrival in New Zealand. *Nature* **598**, 82–85 https://doi.org/10.1038/s41586-021-03858-9 (2021).
21. Eckhardt, S. et al. Revised historical Northern Hemisphere black carbon emissions based on inverse modeling of ice core records. *Nat. Commun.* **14**, 271 https://doi.org/10.1038/s41467-022-35660-0 (2023).
22. Liu, P. et al. Improved estimates of preindustrial biomass burning reduce the magnitude of aerosol climate forcing in the Southern Hemisphere. *Sci. Adv.* **7**, eabc1379 https://doi.org/10.1126/sciadv.abc1379 (2021).
23. Zhang, B. et al. Improved biomass burning emissions from 1750 to 2010 using ice core records and inverse modeling. *Nat. Commun.* **15**, 3651 https://doi.org/10.1038/s41467-024-47864-7 (2024).
24. McConnell, J. et al. Lead pollution recorded in Greenland ice indicates European emissions tracked plagues, wars, and imperial expansion during antiquity. *Proc. Natl Acad. Sci. USA* **115**, 5726–5731 https://doi.org/10.1073/pnas.1721818115 (2018).
25. McConnell, J. R., Lamorey, G. W. & Hutterli, M. A. A 250-year high-resolution record of Pb flux and crustal enrichment in central Greenland. *Geophys. Res. Lett.* **29**, 45–41–45–44 https://doi.org/10.1029/2002GL016016 (2002).
26. Krachler, M., Zheng, J., Fisher, D. & Shotyk, W. Global atmospheric As and Bi contamination preserved in 3000 year old Arctic ice. *Global Biogeochem. Cycles* **23**, GB3011 https://doi.org/10.1029/2009GB003471 (2009).
27. McConnell, J. R., Lamorey, G. W., Lambert, S. W. & Taylor, K. C. Continuous ice-core chemical analyses using inductively coupled plasma mass spectrometry. *Environ. Sci. Technol.* **36**, 7–11 https://doi.org/10.1021/es011088z (2002).
28. McConnell, J. R. et al. Synchronous volcanic eruptions and abrupt climate change ~17.7 ka plausibly linked by stratospheric ozone depletion. *Proc. Natl Acad. Sci. USA* **114**, 10035–10040 https://doi.org/10.1073/pnas.1705595114 (2017).
29. McCrimmon, D., Chellman, N., Wensman, S., Plach, A. & McConnell, J. R. Local variability of ice core ammonium and black carbon records from Tunu and Summit, Greenland: implications for long-term biomass burning reconstructions. *J. Geophys. Res.* **131**, e2025JD046161 https://doi.org/10.1029/2025JD046161 (2026).
30. Sandlos, J. & Keeling, A. *Mining Country: A History of Canada's Mines and Miners* (Lorimer, 2021).
31. Quivik, F. L. *Smoke and Tailings* (Univ. Nevada Press, 2025).
32. MacMillan, D. *Smoke Wars: Anaconda Copper, Montana Air Pollution, and the Courts, 1890–1924* (Montana Historical Press, 2000).
33. McCaskey, H. D. *Mineral Resoures of the United States, 1915: Part I - Metals* (Government Printing Office, 1917).
34. Dunn, E. M. Determination of gases in smelter flues; and notes on the determination of dust losses at the Washoe Reduction Works, Anaconda, Mont. *Trans. Am. Inst. Mining Eng.* **XLVI**, 648–689 (1914).
35. LeCain, T. The limits of "eco-efficiency": arsenic pollution and the Cottrell electrical precipitator in the U.S. copper smelting industry. *Environ. Hist.* **5**, 336–351 https://doi.org/10.2307/3985480 (2000).
36. Atlantic Richfield Company v Gregory A. Christian et al. Number 17-1498. *United States Reports* (US Supreme Court, 1919).
37. White, H. J. Fifty years of electrostatic precipitation. *J. Air Pollut. Control Assoc.* **7**, 166–177 https://doi.org/10.1080/00966665.1957.10467797 (1957).
38. Bowen, H. *Environmental Chemistry of the Elements* (Academic Press, 1979).
39. Stohl, A., Forster, C., Frank, A., Seibert, P. & Wotawa, G. Technical note: the Lagrangian particle dispersion model FLEXPART version 6.2. *Atmos. Chem. Phys.* **5**, 2461–2474 (2005).
40. Eckhardt, S. et al. Source–receptor matrix calculation for deposited mass with the Lagrangian particle dispersion model FLEXPART v10.2 in backward mode. *Geosci. Model Dev.* **10**, 4605–4618 https://doi.org/10.5194/gmd-10-4605-2017 (2017).
41. Bakels, L. et al. FLEXPART version 11: improved accuracy, efficiency, and flexibility. *Geosci. Model Dev.* **17**, 7595–7627 https://doi.org/10.5194/gmd-17-7595-2024 (2024).
42. Hersbach, H. et al. The ERA5 global reanalysis. *Q. J. R. Meteorol. Soc.* **146**, 1999–2049 https://doi.org/10.1002/qj.3803 (2020).
43. Weis, D. et al. High-precision isotopic characterization of USGS reference materials by TIMS and MC-ICP-MS. *Geochem. Geophys., Geosyst.* **7**, Q08006 https://doi.org/10.1029/2006GC001283 (2006).

44. Stock, B. C. et al. Analyzing mixing systems using a new generation of Bayesian tracer mixing models. *PeerJ* **6**, e5096 https://doi.org/10.7717/peerj.5096 (2018).
45. Longman, J. et al. Quantitative assessment of Pb sources in isotopic mixtures using a Bayesian mixing model. *Sci. Rep.* **8**, 6154 https://doi.org/10.1038/s41598-018-24474-0 (2018).
46. Chow, T. J. & Earl, J. L. Lead isotopes in North American coals. *Science* **176**, 510–511 https://doi.org/10.1126/science.176.4034.510 (1972).
47. Díaz-Somoano, M. et al. Stable lead isotope compositions in selected coals from around the world and implications for present day aerosol source tracing. *Environ. Sci. Technol.* **43**, 1078–1085 https://doi.org/10.1021/es801818r (2009).
48. Farmer, J. G., Eades, L. J. & Graham, M. C. The lead content and isotopic composition of British coals and their implications for past and present releases of lead to the UK environment. *Environ. Geochem. Health* **21**, 257–272 https://doi.org/10.1023/A:1006688515919 (1999).
49. Walraven, N., van Os, B. J. H., Klaver, G. T., Baker, J. H. & Vriend, S. P. Trace element concentrations and stable lead isotopes in soils as tracers of lead pollution in Graft-De Rijp, the Netherlands. *J. Geochem. Explor.* **59**, 47–58 https://doi.org/10.1016/S0375-6742(96)00056-8 (1997).
50. Korzeb, S. L. *Interretations of New and Previous Lead Isotopic Data for Late Cretaceous to Eocene Satellite Intrusions, Butte Granite, Volcanic Rocks, and Base Metal Veins of the Boulder Batholith, Southwestern Montana* Bulletin 139, 40 (Montana Bureau of Mines and Geology, 2019).
51. Unruh, D. M., Fey, D. & Church, S. *Chemical Data and Lead Isotopic Compositions of Geochemical Baseline Samples from Streambed Sediments and Smelter Slag, Lead Isotopic Compositions in Fluvial Tailings, and Dendrochronology Results from the Boulder River Watershed, Jefferson County, Montana* Report No. 2000-38 (USGS, 2000).
52. Ulrych, T. J. & Russell, R. D. Gas source mass spectrometry of trace leads from Sudbury, Ontario. *Geochim. Cosmochim. Acta* **28**, 455–469 https://doi.org/10.1016/0016-7037(64)90119-X (1964).
53. Bygnes, L. C. *Emplacement of Metabreccia and Cu-PGE-Rich Sulfide Veins Along the Whistle Offset of the Sudbury Impact Structure*. MSc thesis, Laurentian Univ. (2011).
54. Darling, J. R., Hawkesworth, C. J., Lightfoot, P. C., Storey, C. D. & Tremblay, E. Isotopic heterogeneity in the Sudbury impact melt sheet. *Earth Planet. Sci. Lett.* **289**, 347–356 https://doi.org/10.1016/j.epsl.2009.11.023 (2010).
55. Gray, J. E., Pribil, M. J., Van Metre, P. C., Borrok, D. M. & Thapalia, A. Identification of contamination in a lake sediment core using Hg and Pb isotopic compositions, Lake Ballinger, Washington, USA. *Appl. Geochem.* **29**, 1–12 https://doi.org/10.1016/j.apgeochem.2012.12.001 (2013).
56. Farquhar, R. M. & Haynes, S. J. Lead isotope data for gold-bearing veins and their host metasedimentary rocks of the Goldenville Formation, Eastern Nova Scotia. *Atlantic Geosci.* https://doi.org/10.4138/1599 (1986).
57. Thorpe, R. I., Goodz, M. D., Jonasson, I. R. & Blenkinsop, J. Lead-isotope study of mineralization in the Cobalt district, Ontario. *Can. J. Earth Sci.* **23**, 1568–1575 https://doi.org/10.1139/e86-147 (1986).
58. LeHuray, A. P. *Lead- and Sulfur-Isotope Systematics in Some Sulfide Deposits of the Piedmont and Blue Ridge Provinces of the Southern Appalachians* Report No. 84-112 (USGS, 1984).
59. Peterson, R. E. Lead isotope analysis of native copper deposits in the Lake Superior Basin. *Archaeometry* **66**, 1073–1092 https://doi.org/10.1111/arcm.12962 (2024).
60. Sullivan, M. *Tainted Earth: Smelters, Public Heath, and the Environment* 256 (Rutgers Univ. Press, 2014).
61. Glooschenko, W. A. & Arafat, N. Atmospheric deposition of arsenic and selenium across Canada using sphagnum moss as a biomonitor. *Sci. Total Environ.* **73**, 269–275 https://doi.org/10.1016/0048-9697(88)90435-4 (1988).
62. *Arsenic Chemical Assessment Summary* (US EPA, 1994).
63. *Air Quality Guidelines for Europe* 2nd edn (WHO, 2000).
64. Crump, K. S., Van Landingham, C., Bowers, T. S., Cahoy, D. & Chandalia, J. K. A statistical reevaluation of the data used in the Lanphear et al. (2005) pooled-analysis that related low levels of blood lead tointellectual deficits in children. *Crit. Rev. Toxicol.* **43**, 785–799 https://doi.org/10.3109/10408444.2013.832726 (2013).
65. Richmond-Bryant, J. et al. The influence of declining air lead levels on blood lead–air lead slope factors in children. *Environ. Health Perspect.* **122**, 754–760 https://doi.org/10.1289/ehp.1307072 (2014).
66. McConnell, J. R. et al. Source Data Figures 1–5. *Figshare* https://doi.org/10.6084/m9.figshare.33991051 (2026).
67. Bakels, L. et al. FLEXPART version 11. https://www.flexpart.eu/ (2024).
68. Stock, B. A framework for Bayesian mixing models in R. https://github.com/brianstock/mixsiar (2020).
69. Holland, K. M. et al. Unexpectedly high accumulation rates in the 2022 Mt. Logan ice core reveal warm-season drivers of precipitation variability. *J. Geophys. Res.* **131**, e2025JD044951 https://doi.org/10.1029/2025JD044951 (2026).
70. McConnell, J. R. et al. 20th-century industrial black carbon emissions altered Arctic climate forcing. *Science* **317**, 1381–1384 https://doi.org/10.1126/science.1144856 (2007).
71. Osman, M. B. et al. Abrupt Common Era hydroclimate shifts drive west Greenland ice cap change. *Nat. Geosci.* **14**, 756–761 https://doi.org/10.1038/s41561-021-00818-w (2021).
72. Sigl, M. et al. Timing and climate forcing of volcanic eruptions for the past 2,500 years. *Nature* **523**, 543–549 https://doi.org/10.1038/nature14565 (2015).
73. Opel, T., Fritzsche, D. & Meyer, H. Eurasian Arctic climate over the past millennium as recorded in the Akademii Nauk ice core (Severnaya Zemlya). *Clim. Past* **9**, 2379–2389 https://doi.org/10.5194/cp-9-2379-2013 (2013).

Acknowledgements

Analysis of the ice cores in the array was supported by past NSF and NASA grants, and we acknowledge the students and staff of the DRI ultra-trace ice core laboratory for their assistance. We also thank the NEEM, Akademii Nauk, Mount Logan, Muller Ice Cap and other field teams for their efforts to collect the ice cores; the NSF Ice Core Facility (grant number 2041950) for ice core sampling assistance and curation; and the NSF Ice Drilling Program for support activities through NSF Continuing Grant 2318480. We acknowledge the use of ECMWF's computing and archive facilities provided through a special project (spatvojt). The FLEXPART computational results presented here have been achieved in part using the Vienna Scientific Cluster (VSC). Financial support from the Knut and Alice Wallenberg Foundation (Grant 2023.0253) is gratefully acknowledged.

Author contributions

J.R.M. designed the study, with contributions from N.J.C. and A.S. J.R.M., N.J.C, A.S.C., D.D.-J., D.F. and M.B.O. provided ice samples or previous measurements. J.R.M, N.J.C., S.M.W., A.S.C., K.M.H., D.M. and M.B.O. conducted and analysed measurements. S.M.W. and A.P. conducted model simulations. J.R.M., N.J.C., S.M.W., A.S. and J.S. led the writing of the paper and all other co-authors contributed.

Funding

Collection of the Muller2025-SC intermediate core was supported by University of Alberta start-up funding to A.S.C. and analysis at DRI by NSF grant 2138782 to S.M.W., N.J.C. and J.R.M., as well as grant

2326535 to S.M.W. and N.J.C. Collection of the Logan2022 core was funded by a grant from the National Geographic and Rolex Perpetual Planet Expeditions program to A.S.C., including a supplement to support continuous analysis at DRI. K.M.H. discloses CGS-D support from NSERC.

Competing interests
The authors declare no competing interests.

Additional information
Extended data is available for this paper at https://doi.org/10.1038/s41893-026-01975-9.

Supplementary information The online version contains supplementary material available at https://doi.org/10.1038/s41893-026-01975-9.

Correspondence and requests for materials should be addressed to Joseph R. McConnell.

Peer review information *Nature Sustainability* thanks the anonymous reviewers for their contribution to the peer review of this work. Peer reviewer reports are available.

Reprints and permissions information is available at www.nature.com/reprints.

Publisher's note Springer Nature remains neutral with regard to jurisdictional claims in published maps and institutional affiliations.

Springer Nature or its licensor (e.g. a society or other partner) holds exclusive rights to this article under a publishing agreement with the author(s) or other rightsholder(s); author self-archiving of the accepted manuscript version of this article is solely governed by the terms of such publishing agreement and applicable law.

© The Author(s), under exclusive licence to Springer Nature Limited 2026

https://doi.org/10.1038/s41893-026-01975-9

Extended Data Table 1 | Ice core array details

Core Site	Lat. °N	Lon. °E	Elev. m	Distance to Butte km	Recent Net Snowfall kg/m^2/y	Year Collected	Arsenic Measurement	General References
[c]Tunu2022b	78.0	-33.9	2105	4771	114	2022	Continuous	This study
[a]Summit2023	72.6	-38.3	3258	4674	221	2023	Continuous	This study
Muller2025-SC	79.9	-91.8	1863	3846	273	2025	Continuous	This study
Logan2022	60.6	-140.5	5334	2403	2890	2022	Discrete	69
[a]ACT11d	65.5	-46.3	2148	4402	342	2011	Not measured	2
[a]ACT2	66	-45.2	2408	4455	376	2004	Not measured	1,2
[a]D4	71.4	-43.9	2766	4485	419	2003	Not measured	2,70
[a,b]NUUS2015	70.5	-52.3	2010	4175	~325	2015	Not measured	71
[a]NEEM-2011-S1	77.5	-51.1	2454	4362	207	2011	Not measured	2,72
Akademii Nauk	80.5	94.8	750	5828	460	1999	Not measured	2,73
[c,d]Summit2010	72.6	-38.3	3258	4674	221	2010	Not measured	2,9

[a]Part of the WGC array [b]Antimony not measured [c]Lead isotopes measured on discrete samples [d]Collected within ~500 m of the Summit2023 core.

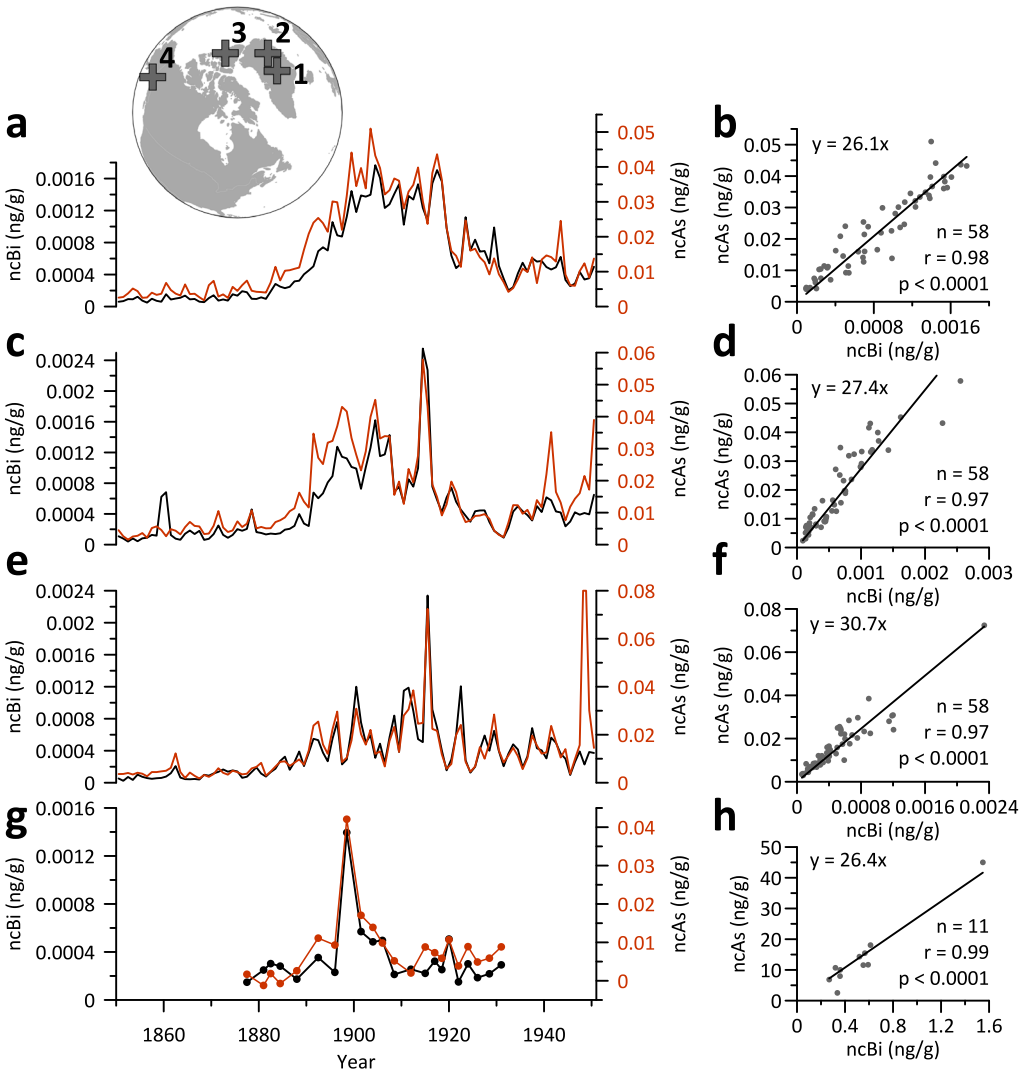
https://doi.org/10.1038/s41893-026-01975-9

Extended Data Table 2 | 1850 to 1950 heavy metal correlations (Pearson's r) in the WGC array

Non-crustal Antimony (ncSb)						
	Summit2023	ACT2	ACT11d	D4	NEEM_2011_S1	NUUS2015
Summit2023	1.00	**0.60**	**0.56**	**0.85**	**0.72**	N/A
ACT2		1.00	**0.37**	**0.57**	**0.57**	N/A
ACT11d			1.00	**0.56**	**0.40**	N/A
D4				1.00	**0.74**	N/A
NEEM_2011_S1					1.00	N/A
NUUS2015						N/A
Non-crustal Bismuth (ncBi)						
-	Summit2023	ACT2	ACT11d	D4	NEEM_2011_S1	NUUS2015
Summit2023	1.00	**0.85**	**0.84**	**0.89**	**0.84**	**0.60**
ACT2		1.00	**0.72**	**0.77**	**0.79**	**0.51**
ACT11d			1.00	**0.76**	**0.76**	**0.48**
D4				1.00	**0.83**	**0.73**
NEEM_2011_S1					1.00	**0.59**
NUUS2015						1.00
Non-crustal Lead (ncPb)						
-	Summit2023	ACT2	ACT11d	D4	NEEM_2011_S1	NUUS2015
Summit2023	1.00	**0.56**	*0.34*	**0.76**	**0.48**	**0.37**
ACT2		1.00	0.22	**0.54**	*0.36*	*0.34*
ACT11d			1.00	*0.35*	0.26	0.21
D4				1.00	**0.51**	*0.35*
NEEM_2011_S1					1.00	0.27
NUUS2015						1.00

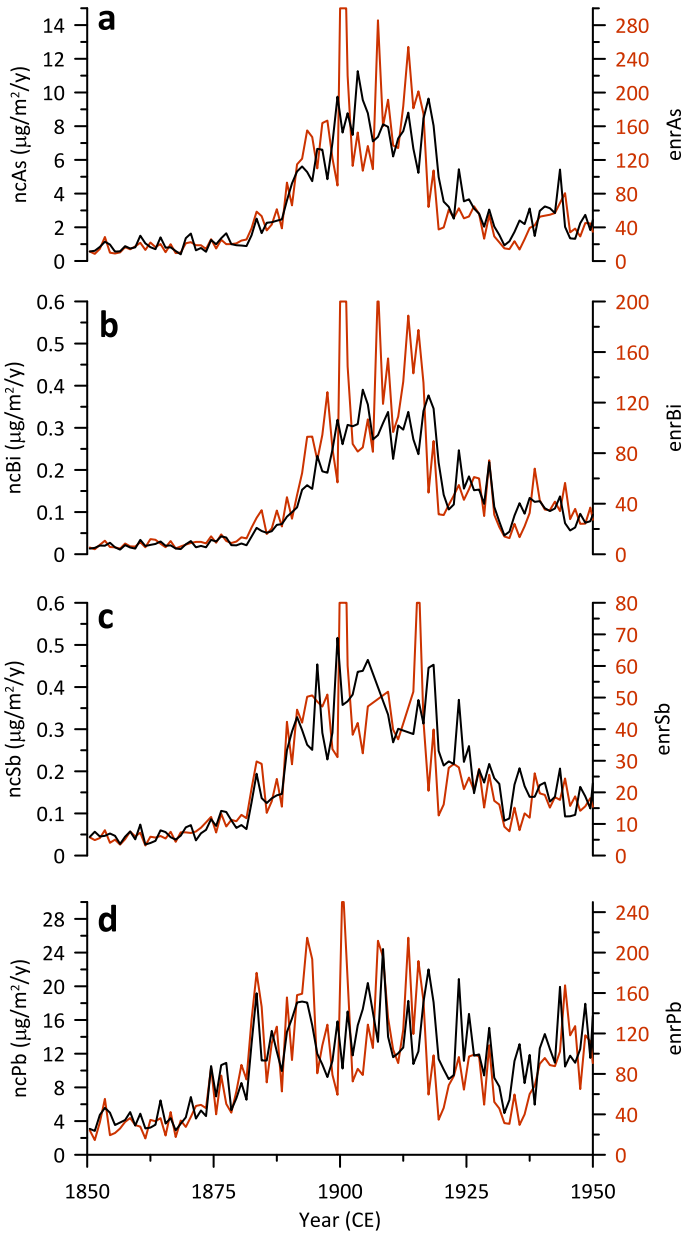
n = 101 ***p* < 0.0001 (one-sided)** *p < 0.001 (one-sided).*

https://doi.org/10.1038/s41893-026-01975-9



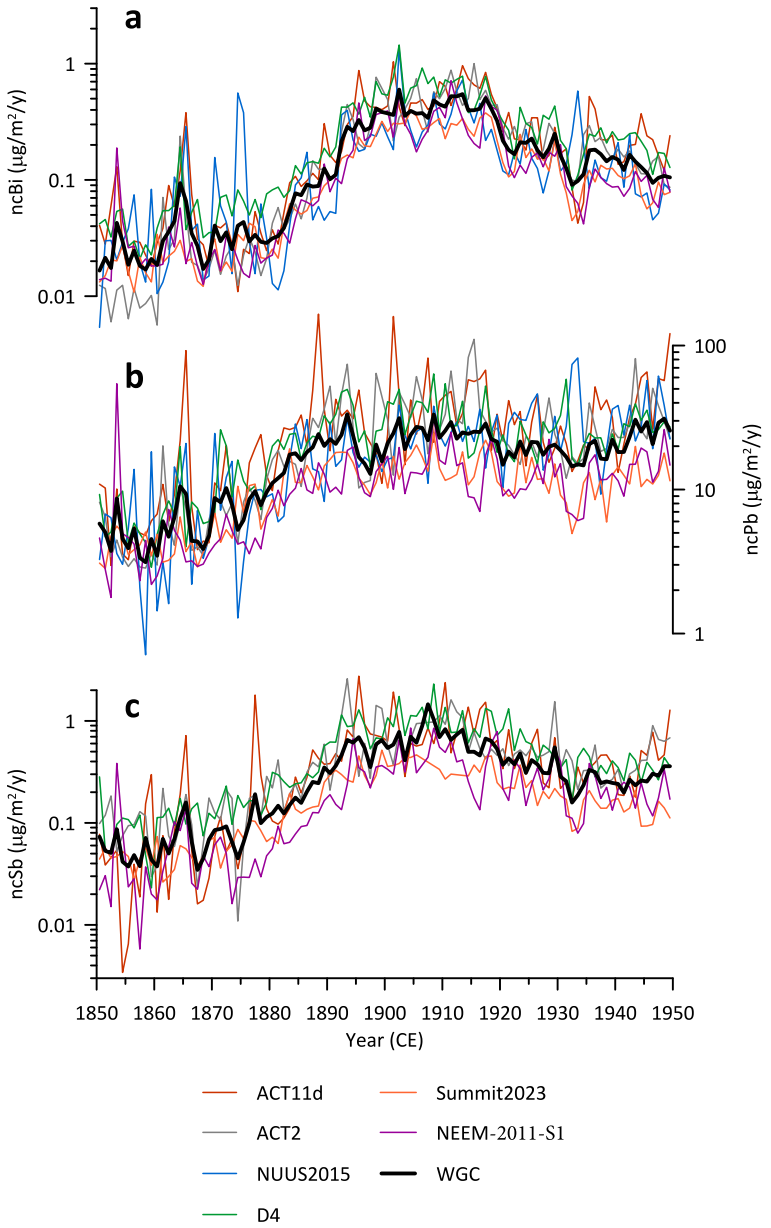
Extended Data Fig. 1 | Co-registered non-crustal arsenic and bismuth concentrations between 1850 and 1950 in four Arctic and near Arctic ice cores. **a**,**b**, Summit2023; **c**,**d**, Tunu2022b; **e**,**f**, Muller2025-SC; **g**,**h**, Logan2022. Cross plots are for 1875 to 1932, and all correlations are highly significant ($p < 0.0001$, one-sided). Inset shows ice core locations: 1. Summit2023, 2. Tunu2022b, 3. Muller2025-SC, 4. Logan2022. Arsenic was measured continuously in Summit2023, Tunu2022b, and Muller2025-SC, and in discrete meltwater samples in Logan2022.

https://doi.org/10.1038/s41893-026-01975-9



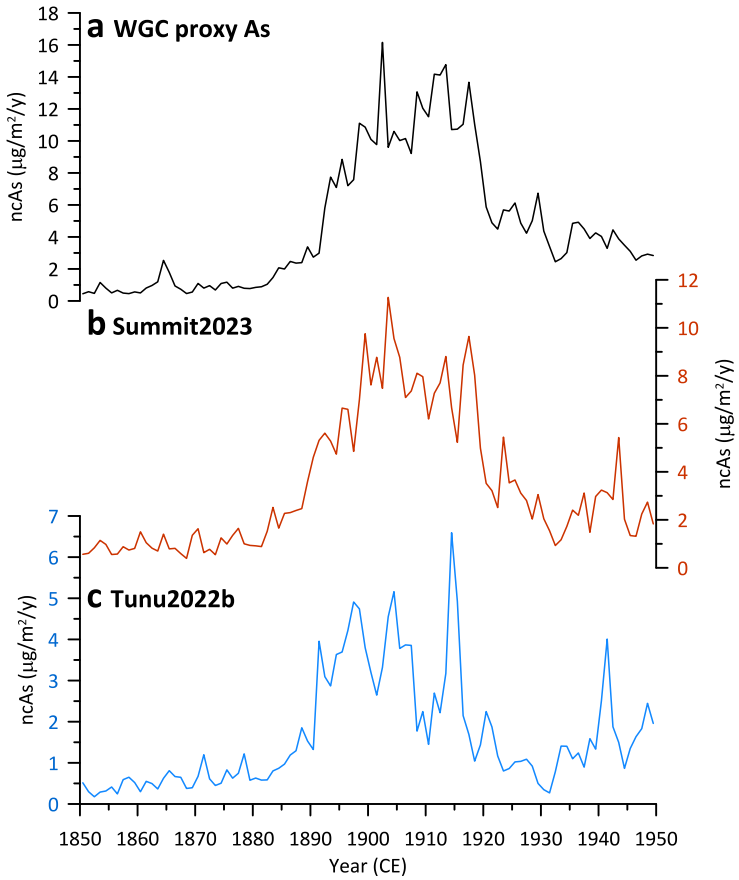
Extended Data Fig. 2 | Annual average non-crustal heavy metal deposition and enrichment relative to cerium (Ce) measured continuously in the Summit2023 core. a, Arsenic. **b**, Bismuth. **c**, Antimony. **d**, Lead.

https://doi.org/10.1038/s41893-026-01975-9



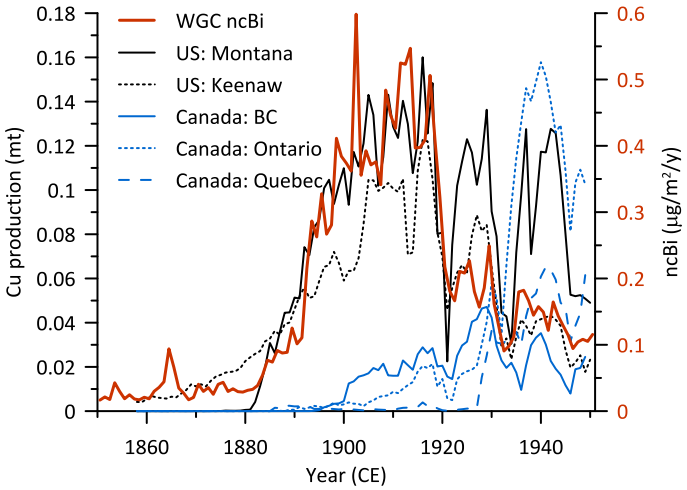
Extended Data Fig. 3 | Individual west Greenland and geometric mean (that is, log average) composite (WGC) records of annual average heavy metal deposition from 1850 to 1950. a, Non-crustal bismuth (ncBi). **b**, Non-crustal lead (ncPb). **c**, Non-crustal antimony ncSb). Note that antimony was not measured in the NUUS2015 core.

https://doi.org/10.1038/s41893-026-01975-9



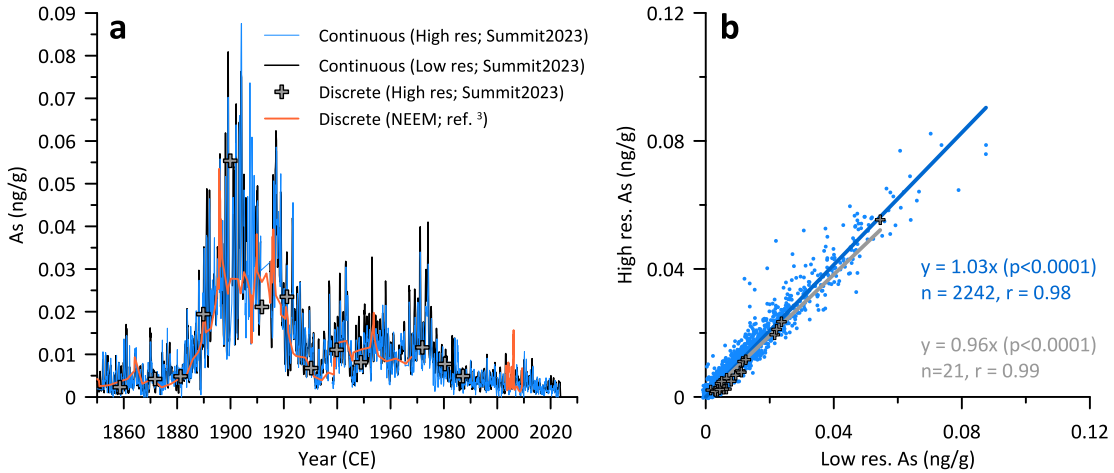
Extended Data Fig. 4 | Comparison of 1850-1950 proxy and measured annual non-crustal As deposition in Greenland. a, WGC proxy ncAs created by log averaging and scaling by 27 (see text) measurements of ncBi in the six west Greenland ice cores including Summit2023. **b**, ncAs measured in the Summit2023 ice core. **c**, ncAs measured in the Tunu2022b ice core from northeast Greenland.

https://doi.org/10.1038/s41893-026-01975-9



Extended Data Fig. 5 | U.S. and Canadian copper production statistics from 1858 to 1950 compared to non-crustal bismuth (as a proxy of non-crustal arsenic) deposition in western Greenland. U.S. Cu production statistics (Butte/Anaconda, Keweenaw) were gleaned from U.S. Geological Survey reports (for example,[33]). Canadian Cu shipment (production not available) statistics are from the Natural Resources Canada and Statistics Canada's Annual Mineral Production Survey. Montana production was almost entirely from the Butte/Anaconda region including the nearby smelter at Great Falls. Note the similar variability and near constant ratio between Montana Cu production and ncBi pollution in Greenland prior to 1919 when the phased installation of Cottrell electrostatic precipitators began with the primary aim of recovering valuable Cu and As from the exhaust fumes and inadvertently decreasing toxic heavy metal emissions. Correlations between WGC ncBi and Montana Cu production following installation of electrostatic precipitators were also highly significant (Fig. 3). Prior to the Great Depression, Ontario base metal production was dominated by Sudbury and British Columbia production by Trail.

https://doi.org/10.1038/s41893-026-01975-9



Extended Data Fig. 6 | Evaluation of arsenic measured using different HR-ICP-MS slit resolutions. a, Continuous and discrete analysis of As in the Summit2023 at different HR-ICP-MS resolutions. Also shown are published discrete As measurements[3] in the NEEM-2009-S1 shallow core that was drilled near the NEEM-2011-S1 core (Extended Data Table 1). **b**, Cross-plot of the Summit2023 measurements with one-sided p values.

nature portfolio

Corresponding author(s): Joseph R. McConnell

Last updated by author(s): September 24, 2026

Reporting Summary

Nature Portfolio wishes to improve the reproducibility of the work that we publish. This form provides structure for consistency and transparency in reporting. For further information on Nature Portfolio policies, see our Editorial Policies and the Editorial Policy Checklist.

Statistics

For all statistical analyses, confirm that the following items are present in the figure legend, table legend, main text, or Methods section.

n/a	Confirmed
☐	☒ The exact sample size (*n*) for each experimental group/condition, given as a discrete number and unit of measurement
☒	☐ A statement on whether measurements were taken from distinct samples or whether the same sample was measured repeatedly
☐	☒ The statistical test(s) used AND whether they are one- or two-sided *Only common tests should be described solely by name; describe more complex techniques in the Methods section.*
☐	☒ A description of all covariates tested
☒	☐ A description of any assumptions or corrections, such as tests of normality and adjustment for multiple comparisons
☐	☒ A full description of the statistical parameters including central tendency (e.g. means) or other basic estimates (e.g. regression coefficient) AND variation (e.g. standard deviation) or associated estimates of uncertainty (e.g. confidence intervals)
☐	☒ For null hypothesis testing, the test statistic (e.g. *F*, *t*, *r*) with confidence intervals, effect sizes, degrees of freedom and *P* value noted *Give P values as exact values whenever suitable.*
☒	☐ For Bayesian analysis, information on the choice of priors and Markov chain Monte Carlo settings
☒	☐ For hierarchical and complex designs, identification of the appropriate level for tests and full reporting of outcomes
☐	☒ Estimates of effect sizes (e.g. Cohen's *d*, Pearson's *r*), indicating how they were calculated

Our web collection on statistics for biologists contains articles on many of the points above.

Software and code

Policy information about availability of computer code

Data collection	Arsenic and other heavy metal data are recorded by the commercially available software for the HR-ICP-MS instruments (Thermo-Fischer).
Data analysis	Simple statistical tests (e.g., r, p-value) and data analyses were performed using Excel or similar commercially available software. As discussed in the manuscript, FLEXPART (version 11) and publicly available ERA5 reanalysis fields were used for atmospheric aerosol and deposition modeling. The Bayesian isotopic mixing model MixSIAR (version 3.1.12) was used to evaluate lead isotopic ratios measured in selected ice cores. All maps were generated using Python's Cartopy and Natural Earth's public domain vector data. This information, as well as links to the FLEXPART, MixSIAR, and Caropy download sites have been included in 'Code availability'.

For manuscripts utilizing custom algorithms or software that are central to the research but not yet described in published literature, software must be made available to editors and reviewers. We strongly encourage code deposition in a community repository (e.g. GitHub). See the Nature Portfolio guidelines for submitting code & software for further information.

Data

Policy information about availability of data

All manuscripts must include a data availability statement. This statement should provide the following information, where applicable:

- Accession codes, unique identifiers, or web links for publicly available datasets
- A description of any restrictions on data availability
- For clinical datasets or third party data, please ensure that the statement adheres to our policy

The ice core data underpinning this research are provided as Source Data so no accession codes are necessary.

Research involving human participants, their data, or biological material

Policy information about studies with human participants or human data. See also policy information about sex, gender (identity/presentation), and sexual orientation and race, ethnicity and racism.

Reporting on sex and gender	N/A.
Reporting on race, ethnicity, or other socially relevant groupings	N/A.
Population characteristics	N/A.
Recruitment	N/A.
Ethics oversight	N/A.

Note that full information on the approval of the study protocol must also be provided in the manuscript.

Field-specific reporting

Please select the one below that is the best fit for your research. If you are not sure, read the appropriate sections before making your selection.

☐ Life sciences ☐ Behavioural & social sciences ☒ Ecological, evolutionary & environmental sciences

For a reference copy of the document with all sections, see nature.com/documents/nr-reporting-summary-flat.pdf

Ecological, evolutionary & environmental sciences study design

All studies must disclose on these points even when the disclosure is negative.

Study description	The aim of this study was to use detailed measurements of highly toxic arsenic and lead in an array of 10 well-dated Arctic ice cores, as well as source tracers, state-of-the-art atmospheric aerosol transport and deposition modeling, historical evidence, and modern epidemiology to evaluate levels, trends, potential emission sources, and possible health impacts before, during, and following the 1870 to 1914 Industrial Revolution.
Research sample	The study included both continuous and discrete elemental measurements in glacier ice samples using the well-established ice core analytical system at the Desert Research Institute. Samples were handled and measurements made using High Resolution Inductively Coupled Plasma Mass Spectrometry following standard procedures.
Sampling strategy	The overall aim was to develop an extensive array of well-dated, accurate records that could be used to (1) quantify spatial and year-by-year temporal patterns of toxic arsenic and lead deposition between 1850 and 1950, (2) identify locations and magnitudes of potential emissions and how and why emissions may have varied, and (3) evaluate possible health impacts. As such, the study primarily leveraged the availability of existing measurements and archived ice core samples to develop a broad spatial array of detailed Arctic and near-Arctic heavy metal pollutant records, including the first detailed array of arsenic records. Ice core samples analyzed continuously were ~1-m longitudinal samples with cross-section ~33 by ~33 mm cut from the cylindrical ice cores. Use of this melter system results in very aggressive decontamination of the longitudinal samples. Discrete samples that were analyzed were captured from the decontaminated meltwater stream from the melter.
Data collection	Arsenic and other heavy metal data are recorded by the commercially available software for the HR-ICP-MS instruments (Thermo-Fischer).
Timing and spatial scale	All ice core measurements were mapped from depth in the glacier or ice sheet to year of deposition using chronologies established for each core. The chronologies were developed using a volcanically constrained annual layer counting following standard procedures. Chronologies for most of the cores have been published previously in peer-reviewed journals (Extended Data Table 1). The very few missing time periods in selected records resulted either from fractured ice that could not be decontaminated properly or availability of no ice in the archive for new measurements of arsenic.

Data exclusions	No data were excluded.
Reproducibility	As detailed in this manuscript and in prior peer-reviewed publications, the ice core heavy metal measurements are highly reproducible.
Randomization	Randomization is not appropriate in ice core chemical measurements.
Blinding	Blinding in general is not appropriate in ice core chemical measurements. That said, to avoid any circular reasoning, the ice core chronologies were developed using annual layer counting of seasonally varying element concentrations of sea salt, continental dust, and biomass burning elements and chemical species, not arsenic, lead, or other heavy metal pollutants evaluated in this study. In addition, volcanic sulfur and tephra fallout was used for volcanic synchronization to constrain the annual layer when necessary.

Did the study involve field work? ☒ Yes ☐ No

Field work, collection and transport

Field conditions	The Arctic and near-Arctic ice cores used in this study were collected from high elevation, very cold (typical mean annual temperatures of -20 to -35 C) alpine glacier sites or from the Greenland Ice Sheet. Samples were transported to the ice core laboratory at the Desert Research Institute at temperatures well below freezing (generally -25 to -10 C) following standard procedures.
Location	Details for each site including latitude, longitude, and elevation are provided in Extended Data Table 1.
Access & import/export	Ice cores were collected in compliance with all local, national, and international laws and permits obtained when necessary.
Disturbance	Efforts were made at all ice coring sites to result in as little disturbance as possible.

Reporting for specific materials, systems and methods

We require information from authors about some types of materials, experimental systems and methods used in many studies. Here, indicate whether each material, system or method listed is relevant to your study. If you are not sure if a list item applies to your research, read the appropriate section before selecting a response.

Materials & experimental systems

n/a	Involved in the study
☒	☐ Antibodies
☒	☐ Eukaryotic cell lines
☒	☐ Palaeontology and archaeology
☒	☐ Animals and other organisms
☒	☐ Clinical data
☒	☐ Dual use research of concern
☒	☐ Plants

Methods

n/a	Involved in the study
☒	☐ ChIP-seq
☒	☐ Flow cytometry
☒	☐ MRI-based neuroimaging

Plants

Seed stocks	N/A.
Novel plant genotypes	N/A.
Authentication	N/A.